

This paper is published as part of a *Dalton Transactions* theme issue:

Dalton Discussion 11: The Renaissance of Main Group Chemistry

Guest Editor: John Arnold
University of California, Berkeley, CA, USA
23 - 25 June 2008

Published in [issue 33, 2008](#), of *Dalton Transactions*

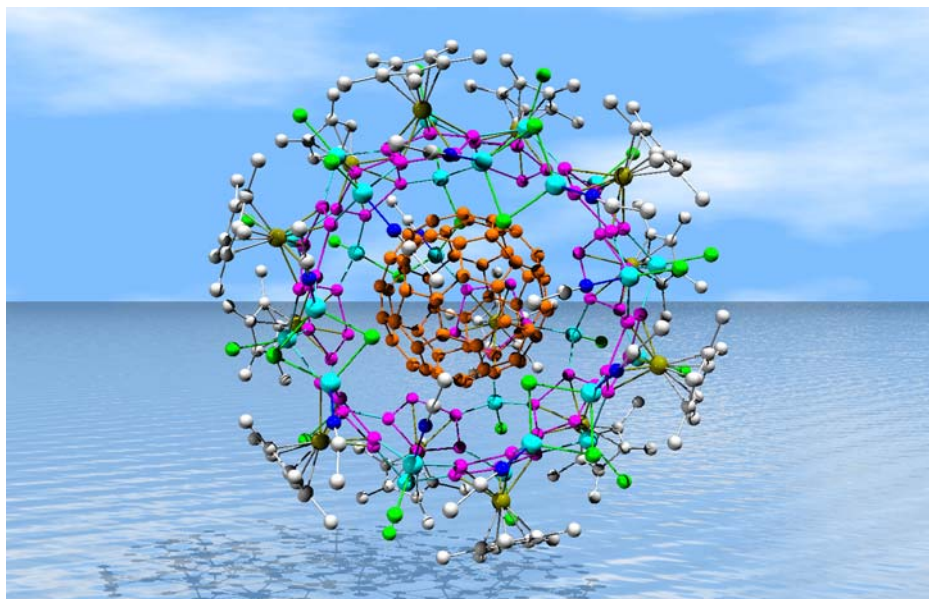


Image reproduced with permission of Manfred Scheer

Papers published in this issue include:

[The coordination chemistry of group 15 element ligand complexes—a developing area](#)

Manfred Scheer, *Dalton Trans.*, 2008 DOI: [10.1039/b718179p](#)

[Formation, structure and bonding of metalloid Al and Ga clusters. A challenge for chemical efforts in nanosciences](#)

Hansgeorg Schnöckel, *Dalton Trans.*, 2008 DOI: [10.1039/b718784j](#)

[Polymeric materials based on main group elements: the recent development of ambient temperature and controlled routes to polyphosphazenes](#)

Vivienne Blackstone, Alejandro Presa Soto and Ian Manners, *Dalton Trans.*, 2008
DOI: [10.1039/b719361k](#)

[Recent developments in the chemistry of low valent Group 14 hydrides](#)

Eric Rivard and Philip P. Power, *Dalton Trans.*, 2008 DOI: [10.1039/b801400k](#)

[Chemistry and physics of silicon nanowire](#)

Peidong Yang, *Dalton Trans.*, 2008 DOI: [10.1039/b801440j](#)

Visit the *Dalton Transactions* website for more cutting-edge inorganic and organometallic research
www.rsc.org/dalton

Materials for hydrogen storage: structure and dynamics of borane ammonia complex†‡

Vencislav M. Parvanov,^a Gregory K. Schenter,^a Nancy J. Hess,^a Luke L. Daemen,^b Monika Hartl,^b Ashley C. Stowe,^a Donald M. Camaioni^a and Tom Autrey^{*a}

Received 23rd November 2007, Accepted 7th February 2008

First published as an Advance Article on the web 14th July 2008

DOI: 10.1039/b718138h

The activation energies for rotations in low-temperature orthorhombic ammonia borane were analyzed and characterized in terms of electronic structure theory. The perdeuterated ¹¹B-enriched ammonia borane, ¹¹BD₃ND₃, sample was synthesized, and the structure was refined from neutron powder diffraction data at 175 K. This temperature has been chosen as median of the range of previously reported nuclear magnetic resonance spectroscopy measurements of these rotations. A representative molecular cluster model was assembled from the refined geometry, and the activation energies were calculated and characterized by analysis of the environmental factors that control the rotational dynamics. The barrier for independent NH₃ rotation, $E_a = 12.7$ kJ mol⁻¹, largely depends on the molecular conformational torsion in the solid-state geometry. The barrier for independent BH₃ rotation, $E_a = 38.3$ kJ mol⁻¹, results from the summation of the effect of molecular torsion and large repulsive intermolecular hydrogen–hydrogen interactions. However, a barrier of $E_a = 31.1$ kJ mol⁻¹ was calculated for internally correlated rotation with preserved molecular conformation. Analysis of the barrier heights and the corresponding rotational pathways shows that rotation of the BH₃ group involves strongly correlated rotation of the NH₃ end of the molecule. This observation suggests that the barrier from previously reported measurement of BH₃ rotation corresponds to H₃B–NH₃ correlated rotation.

Introduction

Recently, ammonia borane (AB) with 19 mass% hydrogen has received much attention as a material to store hydrogen for fuel cell applications.¹ However, this hydrogen-rich complex has been a scientific curiosity for both experimentalists and theorists beginning with its synthesis and characterization more than 50 years ago.² The BH₃–NH₃ molecule is a classic example of a donor–acceptor complex.³ The non-bonding electrons from the nitrogen p-orbital occupy an empty p-orbital of the boron and form a dative bond. This yields a molecule with dipole moment of 5.1 D⁴ and polarization of the hydrogen atoms attached to the electron-deficient nitrogen and the electron-rich boron. The intermolecular electrostatic attraction between protonic N–H and hydridic B–H ends of adjacent molecules in the solid state was examined recently by Klooster *et al.*⁵ They measured the neutron diffraction pattern of a single crystal AB at 200 K and showed close contacts (2.0–2.2 Å), less than the sum of the van der Waals radii (2.4 Å), between adjacent protonic and hydridic hydrogen atoms. This specific interaction, where the hydridic B–H is a hydrogen

bond acceptor to the protonic N–H hydrogen bond donor, is referred to as “dihydrogen bonding.” Later, Morrison and Siddick used density functional theory (DFT) and calculated a cohesive energy of 76 kJ mol⁻¹ for the six dihydrogen bonds, per molecule in the crystal.⁶ Alternatively, a value of 97 kJ mol⁻¹ is estimated from the standard heats of formation of AB in solid and gaseous states.⁷ Such a large molecular cohesive energy is consistent with the low vapor pressure observed for solid AB, <1 micron at 300 K.⁸ These specific dihydrogen bonding interactions are of interest to many research groups in their search for properties that lead to low temperature release of chemisorbed hydrogen.⁹ Our goal is to develop better fundamental insight into the effect of dihydrogen bonding on the chemical and physical properties of AB. In this article, we discuss our work to study how the intermolecular interactions between the BH₃ and NH₃ groups of adjacent molecules affect the rotation about the B–N dative bond of AB in the solid phase.

The barrier of 8.5 kJ mol⁻¹ for rotation about the B–N bond of AB determined from gas-phase microwave spectroscopy⁴ is slightly less than the corresponding barrier of 12.6 kJ mol⁻¹ for rotation about the C–C bond in ethane.¹⁰ Calculations at different levels of electronic structure theory in the gas phase for both isoelectronic molecules, H₃C–CH₃ and H₃N–BH₃, have shown that this rotational barrier is a result of the transition from the stable “staggered” to “eclipsed” conformation (S → E). In AB, the barrier depends on the length of the B–N bond and is dominated by Pauli repulsion effects;^{11,12} while for ethane, responsible is the stabilizing hyperconjugative interaction.¹² Experimental studies

^aFundamental and Computational Sciences Directorate, Pacific Northwest National Laboratory, Richland, WA, 99352, USA. E-mail: tom.autrey@pnl.gov; Fax: 1-509-375-6660; Tel: 1-509-375-3792

^bLos Alamos National Laboratory, Los Alamos, NM, 87545, USA

† Based on the presentation given at Dalton Discussion No. 11, 23–25 June 2008, University of California, Berkeley, USA.

‡ Electronic supplementary information (ESI) available: Structural parameters from NPD refinement at 175 and 200 K. See DOI: 10.1039/b718138h

have shown that in the solid phase, the B–N bond of AB is shorter (1.587 Å),⁵ than in the gas phase (1.672 Å-effective; 1.658 Å-isotope substituted).⁴ This significant decrease in the bond length alone might be expected to increase the rotational barrier due to increased exchange repulsion (EX) interactions.^{11,12} However, there are other factors, *i.e.*, dihydrogen bonding, dipole–dipole, and lattice interactions that may also influence the rotational dynamics of AB in the solid state. Structural studies have found an order–disorder phase transition at 225 K with a tetragonal unit cell above and orthorhombic below this temperature.¹³ For both phases Reynhardt and Hoon¹⁴ have suggested dynamic site exchange of equivalent hydrogen atomic positions or reorientation of NH₃ and BH₃ in the crystal. Using selective deuteration (ND₃BH₃ and NH₃BD₃), Penner and coworkers described these motions as rotations with potential barriers determined by intermolecular interactions in the crystal.¹⁵ Measurements from these nuclear magnetic resonance spectroscopy (NMR) T₁ spin lattice relaxation experiments of ¹H, ²H, and ¹⁵N in addition to ²H line shape analysis have shown that BH₃ and NH₃ groups in solid AB have rotational barriers that are different from each other as well as different from the barrier for conformational torsion in the gas phase.^{14–16} In the tetragonal phase and temperatures between 225 and 300 K, Penner and coworkers reported barriers of 5.9 and 7.3 kJ mol^{−1} for BD₃ and ND₃, respectively. Based on the similar values of the barriers measured for BD₃ and ND₃ and the fact that both are lower than the value of the gas phase torsional barrier (8.5 kJ mol^{−1}), Penner *et al.* concluded that there is a “whole molecule” rotation in this phase. In the orthorhombic phase and at temperatures between 115 and 225 K, they reported barriers of 26 and 13.7 kJ mol^{−1} for BD₃ and ND₃, respectively. Because of the significant difference between the NH₃ and BH₃ rotational barriers, Penner *et al.* concluded that in the orthorhombic phase, these groups rotate independently.

These experimental studies provide a quantitative comparison between gas-phase and solid-phase rotational barriers and establish very important basis for understanding of the dynamics in crystal AB. The experiment of selective isotopic labeling (BH₃–ND₃, BD₃–NH₃, BH₃–¹⁵NH₃)^{14,15} measures the barriers of BD₃ and ND₃ (or ¹⁵NH₃) rotations separately. However, it is not possible to measure these rotations completely unaffected by correlated motions. Theoretical modeling is instrumental to investigate possible correlated motions and help understand the experimental results. With an appropriate model, it is possible to examine the environmental factors that control the rotational dynamics in the solid state of AB. In this work, we present a relevant theoretical model with geometry parameters obtained from refinement of structural data of ¹¹BD₃ND₃ at 175 K from neutron powder diffraction (NPD) experiment.¹⁷ We describe the computational approach and examine the fundamental interactions involved in the rotation of the BH₃ and NH₃ groups in the orthorhombic phase of AB. The rotational barriers obtained from the model agree qualitatively and quantitatively with the NMR results from the experimental measurements. Furthermore, the theoretical modeling approach provides insight into the mechanisms controlling the rotational dynamics by determination of the contributions from (1) the intrinsic molecular barrier for conformational rotation about the H₃N–BH₃ bond in the solid state, (2) the interactions between nearest neighbors (*i.e.*, dihydrogen), and (3) lattice interactions and the collective motions in the molecular crystal.

Experimental

Synthesis of ¹¹BD₃ND₃

In order to obtain resolution in the NPD pattern of AB, the isotopically labeled ¹¹BD₃ND₃ material was synthesized by a multi-step route using a series of procedures available in the literature. Given the absence of commercial availability of NaD, multiple steps were required to incorporate deuterium on to the ¹¹B-enriched AB. A brief summary with references is provided.

Na¹¹BH₄. Boron-11 labeled boric acid (¹¹B(OH)₃), Eagle-Picher, was dissolved in excess anhydrous methanol to yield a ¹¹B(OCH₃)₃ methanol solution. The methanol-trimethylborate azeotrope was recovered by fractional distillation (vapor temperature 49 °C). The methanol-trimethylborate azeotrope was then broken by addition of excess LiCl.¹⁸ The pure trimethylborate is recovered with a separatory funnel. ¹¹B NMR and Fourier transform infrared spectroscopy (FTIR) confirmed the product purity. In the next step, the ¹¹B(OCH₃)₃ was added slowly dropwise over a period of 2 h to 9 equivalents of NaH at 250 °C with mechanical stirring under a nitrogen atmosphere. Upon completion, the reaction flask was allowed to cool to ambient temperature. Isopropylamine was used to extract the soluble borohydride products and recrystallization yields Na¹¹BH₄.^{17b}

Na¹¹BD₄. Na¹¹BH₄ and (CH₃)₃NHCl were added to tetrahydrofuran (THF) at 30 °C and allowed to stir for 8 h under an argon atmosphere. The reaction liberated 1 mol of hydrogen gas, and a white solid, (CH₃)₃N¹¹BH₃, was obtained after filtration and recrystallization.¹⁹ This borane species was synthesized based on the fact that it is the only amine-borane compound that does not undergo immediate dehydrogenation when introduced to acid and allows for the H-to-D exchange on boron. In the next step, (CH₃)₃N¹¹BH₃ in solution in Et₂O (approximately 1 M) was added to a 0.6M DCl solution in D₂O. The heterogeneous mixture was stirred vigorously for 2 h.²⁰ The trimethylamine-borane was recovered by extraction with diethyl ether (Et₂O) in a separatory funnel and then dried over anhydrous K₂CO₃. Et₂O was removed on the rotary evaporator at room temperature to yield >95% deuteration of the hydride atoms bound to boron as confirmed by infrared spectroscopy (IR) and ¹H NMR spectroscopy. Finally, to a solution (CH₃)₃N¹¹BD₃ dissolved in anhydrous diglyme were added equimolar quantities of NaOCH₃. The reaction was stirred for 8 h under an argon atmosphere. The exchange reaction resulted in the liberation of (CH₃)₃N gas and formation of polycrystalline Na¹¹BD₄ upon removal of solvent. Purity and isotopic composition was confirmed by IR and ¹¹B NMR.

¹¹BD₃ND₃. Na¹¹BD₄ was mixed with one equivalent of ammonium formate in THF and sonicated (300 W) for 30 min. Filtration and solvent removal under vacuum yielded white polycrystalline ¹¹BD₃NH₃ (80% yield). Deuteration of the amine protons was achieved by dissolving ¹¹BD₃NH₃ in excess of D₂O.²¹ After three deuteration cycles, less than 1% protons were present in AB.

NPD measurements of ¹¹BD₃ND₃

The diffraction experiments were conducted at the Los Alamos Neutron Science Center's Manuel Lujan Jr. Neutron Scattering Center (LANSCE) on the neutron powder time-of-flight

diffractometer for a deuterated $^{11}\text{BD}_3\text{ND}_3$ powder sample. The $^{11}\text{BD}_3\text{ND}_3$ powder (0.5 gm) was loaded into a vanadium can under an argon atmosphere to prevent water molecules from absorbing in the powder. The sample can was attached to a displax closed cycle refrigerator and the temperature was set at 175 K and controlled using a K-type thermal couple to ± 1 K of the desired temperature. The neutron beam was moderated using chilled water. The crystal structure was refined from the NPD data collected at over four detector banks covering a momentum transfer range from 0.8 to 42 \AA^{-1} . Using the Rietveld method,²² as implemented in the Generalized Structure and Analysis Software (GSAS) package with EXPGUI interface (National Institute of Standards and Technology),²³ the refinements were performed in the $Pmn2_1$ space group for the orthorhombic structure. The 200 K structure reported by Klooster *et al.*⁴ was used as a starting point for the 175 K data set. The time-of-flight (TOF) profile function used was based on one developed by David and Von Dreele (unpublished) to describe the leakage of fast and slow neutrons from the moderator. It consists of the Ikeda-Carpenter function convolved with a pseudo-Voigt function. The refinements included the scale factor, zero, background, the unit cell parameters, peak shape function, atomic fractional coordinates, and thermal parameters. A shifted Chebyshev polynomial with 12 to 25 terms, depending on the complexity of the background, was used as the basis for the background function. All thermal parameters were initially treated as isotropic for the initial rounds of refinement and then were allowed to be anisotropic. Finally, the occupancies of H and D were refined.

Development of the model and computational details

A molecular cluster representing the nearest neighbor crystal environment was developed to simulate the immediate interactions and estimate the barriers for rotations of BH_3 and NH_3 in AB. This approach allows examination of the rotations unaffected by possible artificially correlated motions that could be introduced by applying periodic boundary conditions to a small system. The structural data from the NPD refinement at 175 K was used to construct a representative cluster of 9 molecules in a crystal arrangement 1.4 times the size of the unit cell. The cluster model consists of one molecule in the center of the all 8 first neighbors (cage) interconnected with dihydrogen bonds. The central molecule was symmetrized to C_{3v} point group by averaging the geometric parameters of the hydrogen atoms of each end group—the bond lengths as well as the angles with respect to the B–N bond. A potential energy surface (PES) for rotation of the BH_3 and NH_3 groups of the central molecule was then obtained by calculating the electronic energies of the configurations generated by rotating the hydrogen atoms about the B–N axis. The rotation was performed over the range $0 \leq \theta_{\text{NH}_3} \leq 120^\circ$ and $0 \leq \theta_{\text{BH}_3} \leq 120^\circ$ in 10° increments with respect to the initial positions. The boron and nitrogen of the symmetrized central molecule and all 8 neighbors including hydrogen were kept in their positions from the refinement. Thus, a total of 169 configurations were calculated to give the energy as a function of the rotational angles θ_{NH_3} and θ_{BH_3} . The energies were calculated using DFT with the hybrid B3LYP²⁴ functional and 6-31++G** basis set.²⁵ This set of calculations was performed without optimization of the geometric parameters using Gaussian 98.²⁶ The PES was transformed to a representation

of relative energies, by subtracting the energy of the point of the initial position (minimum) from the energies of each point of the surface or $\Delta E = E(0 \leq \theta_{\text{BH}_3} \leq 120; 0 \leq \theta_{\text{NH}_3} \leq 120) - E(\theta_{\text{NH}_3} = 0; \theta_{\text{BH}_3} = 0)$. The energies of the maxima and the saddle point on the relative PES represent barriers or activation energies (E_a).

Energies of the barriers were calculated at MP2/6-31++G** level of theory with no optimization. Alternatively, the barriers were calculated by a set of optimizations at B3LYP/6-31++G** level of theory. Two sets of optimizations with an increasing number and degrees of freedom of hydrogen atoms were performed to calculate the respective barriers. No search for transition state (in terms of a single imaginary frequency) was performed for both sets of optimization runs. In a fixed boron and nitrogen system, first only hydrogen atoms involved in dihydrogen bonding were allowed to relax. In the second optimization set, all hydrogen atoms in the 9-molecule cluster were allowed to relax with restriction of a single dihedral angle of the central AB. This angle was chosen to control the orientation of the central molecule with respect to the initial positions, but the model allows all B–H and N–H bonds and molecular bond angles in the cluster to relax.

The energies of interaction of the central molecule with the 8 surrounding neighbors in the barrier configurations were analyzed using energy decomposition analysis (EDA). The method employed for this analysis, in the scheme introduced by Morokuma and coworkers, is implemented in the GAMESS software.²⁷ The implementation is restricted to Hartree–Fock method and the applied level of theory of these calculations was HF/6-31G.

Results and discussion

The structure of AB was determined at 175 K using isotopically-labeled $^{11}\text{BD}_3\text{ND}_3$ and NPD refinement technique (file with the structural parameters is provided in the ESI).[‡] The structure is represented by an orthorhombic unit cell similar to the single crystal neutron diffraction structure obtained by Klooster *et al.*⁵ for undeuterated, unenriched AB sample at 200 K. A slight difference is the change in the parameters of the unit cell (a comparison of the geometry parameters is made in Table S1[‡] in the ESI) and the angle of deviation of the B–N bonds from the parallel with the c axis. In the tetragonal unit cell (above 225 K) all B–N bonds are parallel to the c axis. With the phase transition to orthorhombic unit cell (below 225 K), the boron and nitrogen positions are shifted in opposite directions along c and b axes; thus, the B–N bonds deviate from the parallel to the c axis. The angle of deviation increases in b direction from 8.0 at 200 K to 10.0° at 175 K.²⁸ In Fig. 1a (a view along the a axis), this specific feature of the orthorhombic phase at 175 K is illustrated as layers of oppositely tilted B–N bonds. Due to this tilting, the trajectories of rotation of the hydrogen atoms about the B–N bonds overlap non-planar dihydrogen networks. A slice parallel to a dihydrogen network and representing fragments of AB molecules (top down view) forming dihydrogen bonds is shown in Fig. 1b. This representation shows the geometry of the surroundings along the rotational trajectories for BH_3 and NH_3 groups. Each BH_3 group is surrounded by four NH_3 groups from neighboring AB molecules and *vice versa*. The figure shows that 3 out of 4 distances between closest hydrogen atoms from the BH_3 groups surrounding one NH_3 (Fig. 1b, 2H–2H and 1H–2H distances) are shorter than the corresponding distances between closest hydrogen atoms from

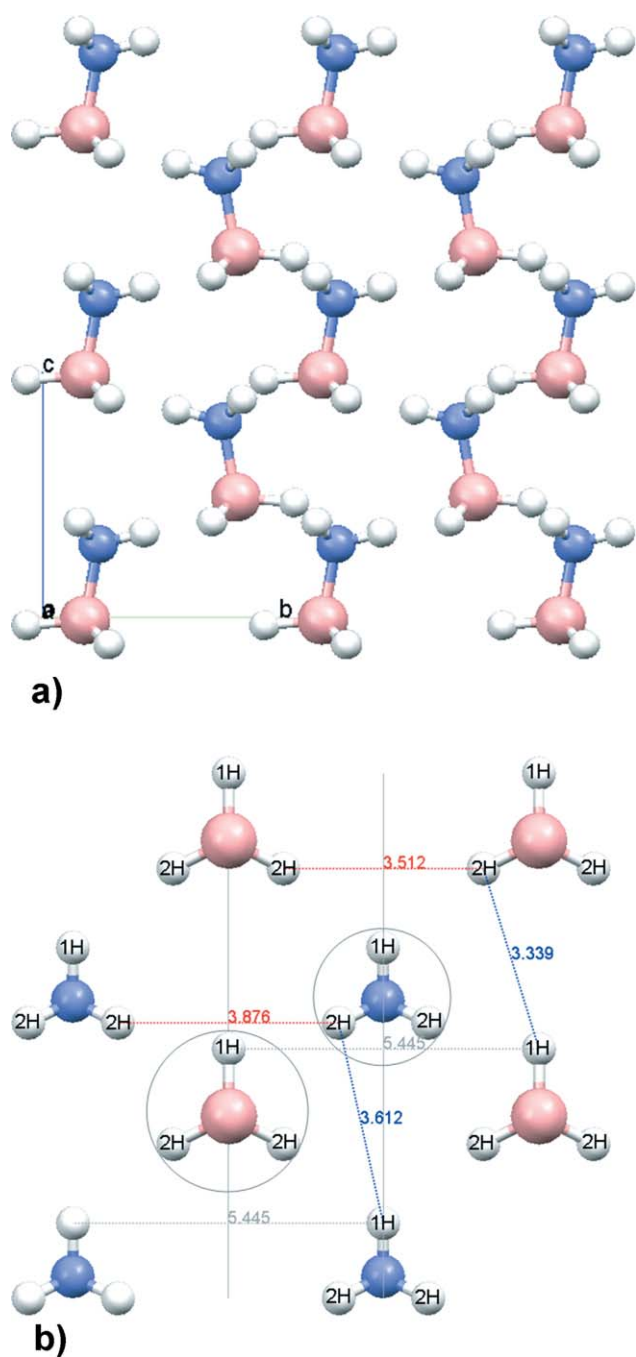


Fig. 1 (a) Representation of fragment of ammonia borane at 175 K, corresponding to 2.4 times the size of the unit cell refined from NPD of $^{11}\text{BD}_3\text{ND}_3$. The view corresponds to orientation along a axis; (b) Fragments of ammonia borane molecules forming dihydrogen network represented in a slice in c direction and 2.0 by 2.0 times of a and b of the unit cell. 1H and 2H annotations represent the position with respect to the molecular mirror plane along b direction. The colors of atoms are as follows: H—white, N—blue, B—beige-red.

the NH_3 groups surrounding one BH_3 . The B–H–H–B distances are shorter than the corresponding N–H–H–N distances due to the molecular geometry of AB, specifically longer H–B than H–N bonds. Molecular geometry parameters are provided in Table S1 of the ESI.† The difference in the geometry of the rotational

surrounding of BH_3 and NH_3 suggests non-equivalent rotational conditions. The intermolecular distances and the corresponding geometry of the surrounding are related to the change of the dihydrogen bonding along the rotational trajectory. The effect of the dihydrogen bond lengths on the barriers of rotation is discussed in detail later in the text. The effect of the molecular geometry including the B–N bond length, which was found in previous studies^{11,12,30} to influence the barrier of molecular torsion, was also taken into account. In the crystal at 175 K, the B–N bond of AB is 1.568 Å, which is shorter compared to the reported gas-phase bond length (1.672 Å—effective; 1.658 Å—*isotope substituted*).⁴ In a following section discussing the components of the total rotational potential in the crystal, the molecular torsion in the geometry of the molecule in the crystal is estimated and considered as a contribution to the rotational barriers.

Energy profiles of the rotational motions

As described in the section on computational methods, electronic structure calculations were performed for rotation of BH_3 and NH_3 groups of an AB molecule inside a cluster model of solid AB at 175 K. Fig. 2 shows the configurations corresponding to the minimum (**I**), the maxima (**II** and **IV**), and the saddle point (**III**) on the PES (in Fig. 3a). The images in Fig. 2 also represent rotations that interchange the positions of hydrogen atoms of the central AB molecule. Rotation of one of the ends of the central AB molecule with the opposite end fixed in its initial position ($0 \leq \theta_{\text{NH}_3} \leq 120$ when $\theta_{\text{BH}_3} = 0$ and *vice versa*) is equivalent to an independent or uncorrelated rotation. Thus, in Fig. 3a, the curves defining the edges of the 3D plot of the relative PES correspond to energy profiles of the uncorrelated BH_3 and NH_3 rotations. Such rotations include molecular staggered to eclipsed (S \rightarrow E) conformational torsion of the central AB ($\Delta\theta = \theta_{\text{NH}_3} - \theta_{\text{BH}_3}$; $0 \leq \Delta\theta \leq 60$), where the staggered conformation is energetically preferred (favorable) compared to the eclipsed one. In the initial position **I** (Fig. 2), the BH_3 and NH_3 groups are in their lowest energy (as defined by the structural refinement) orientations with respect to each other (staggered conformation) and with respect to the surrounding neighbors. In **II** (Fig. 2), the NH_3 group is rotated from its initial position such that it eclipses the BH_3 group in its initial position. Whereas in **IV** (Fig. 2) is the opposite; the BH_3 group is rotated from its initial position such that it eclipses the NH_3 group in its initial position. Alternatively, a rotation of the entire central molecule with fixed torsional angle ($\Delta\theta$) to preserve the molecular conformation is equivalent to fully correlated rotation of the BH_3 and NH_3 groups. In **III** (Fig. 2), the central AB is in staggered conformation ($\Delta\theta = 0$) like in configuration **I**, only both ends are rotated at 60° with respect to the surrounding neighbors. This configuration corresponds to the saddle point **III** (Fig. 3a) on the relative PES. Thus, the saddle point is the maximum of the energy pathway of the correlated rotation shown as a line from **I** to **III** in Fig. 3a.

The calculated barrier for uncorrelated NH_3 rotation of 12.7 kJ mol^{-1} in **II** is in very good agreement with the experimental value (13.7 kJ mol^{-1})¹⁵ and significantly smaller than the uncorrelated BH_3 barrier of 38.3 kJ mol^{-1} in **IV** (Table 1). Although the calculated uncorrelated BH_3 rotational barrier is much higher than the measured value for this rotation of 26 kJ mol^{-1} ,¹⁴ the calculated values are in agreement with the experimental

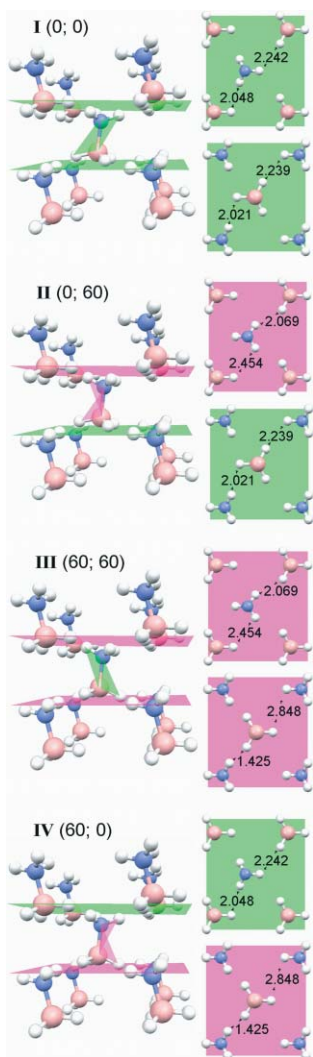


Fig. 2 Cluster in geometries of rotation of the central BH_3 and NH_3 groups about the B–N bond (θ_{BH_3} ; θ_{NH_3} in parentheses) and views along central B–N of immediate neighbors with closest distances.

findings of significant difference between the two barriers.^{14,15,16} Furthermore, we note that the correlated BH_3 – NH_3 rotational barrier (31.1 kJ mol^{-1}) in **III** is lower than the uncorrelated one and closer to that measured for BH_3 (difference of 5.1 kJ mol^{-1} or about $1.2 \text{ kcal mol}^{-1}$). This energy difference with the measured is small and is within the limit of the accuracy of the calculation. The rotation pathway through point **III** in Fig. 3a, corresponding to the maximum of correlated BH_3 – NH_3 rotation, is a lower energy pathway than the one through point **IV** corresponding to the maximum of uncorrelated BH_3 rotation. The saddle point **III** is 7 kJ mol^{-1} downhill from the uncorrelated BH_3 maximum in **IV**. This suggests that the minimum energy path (MEP) of BH_3 rotation goes through **III** rather than **IV**. In Fig. 4, the relative PES is extended to a full rotation range of 360° for θ_{NH_3} and θ_{BH_3} and provides a better view of **IV** as the highest point. Thus, any trajectory going through **IV** cannot correspond to an energy-efficient rotational pathway. The MEP predicted by this model then corresponds to rotation of BH_3 , concurrent with NH_3 rotation, to preserve the staggered conformation of the central molecule. Such an energy path can be explained with internal

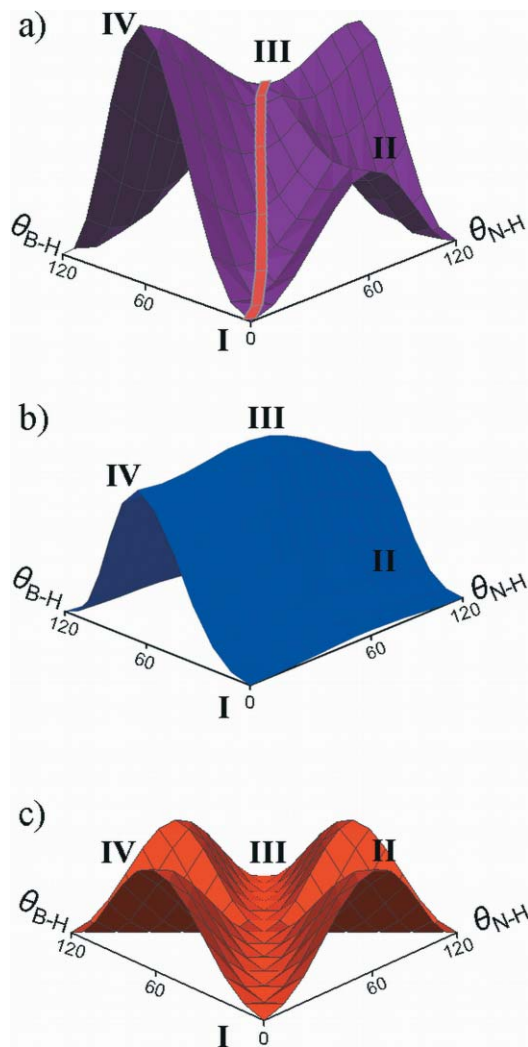


Fig. 3 Relative PES from energies as function of rotational angles and the corresponding extrema **I** \rightarrow **IV**: (a) total energy with correlated rotational pathway ($\Delta=0$ marked in red); (b) intermolecular interactions; (c) conformational torsion of the central AB.

Table 1 Relative activation energies, E_a , or barrier as difference with $E(\mathbf{I})$; interaction energy of the central molecules with the neighbors $-IE$; the difference $\Delta IE = IE(\mathbf{I} \rightarrow \mathbf{IV}) - IE(\mathbf{I})$; E_a -opt are for relaxed central hydrogen, dihydrogen bonds (di H), and all hydrogen (all H). For both B3LYP and MP2 methods, the 6-31++G** basis set was used. All energies are given in kJ mol^{-1}

	B3LYP		ΔIE	E_a -opt		MP2 E_a
	E_a	IE		di H	all H	
II	12.73	−6.11	1.20	15.11	14.86	12.67
III	31.08	23.78	31.08	34.01	35.57	36.03
IV	38.29	19.46	26.76	—	—	44.75

molecular forces that prevail over the stabilization intermolecular interactions at the NH_3 end of the central molecule (Fig. 2, **IV**) and, thus, lead to a correlated BH_3 – NH_3 rotation.

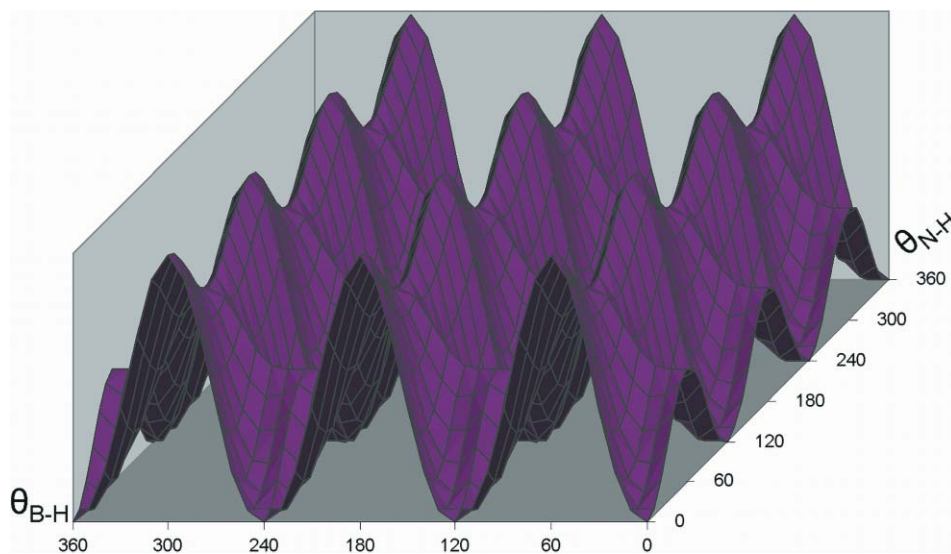


Fig. 4 Relative PES extended to 360° of rotation.

Molecular and environmental components of the PES

The energy profiles rule out the uncorrelated BH_3 rotation (through **IV** on the PES) and suggest competition between internal molecular forces and the intermolecular interactions. This competition was examined by analysis of the components forming the rotational potentials and the respective barriers. The heights of the calculated barriers can be understood through analysis of the contributions from (1) the effect of the internal molecular interactions due to the conformational torsion of the central AB and (2) the interaction of the rotating central AB with the surrounding molecules. We have noted that the geometry of AB molecule in the solid is different from the gas phase with shorter B–N bond; thus, the effect of the crystal environment on the molecular structure affects also the internal conformational torsion. The molecular and environmental effects are interconnected in the solid state, but the aim of the approach in this study is to separate these effects and compare the specific contributions to the rotational barriers.

The molecular and environmental interactions were expressed as components of the potential energy of the cluster as follows. The 9-molecule cluster was separated into two fragments, first consisting of the central AB and second the cage of 8 neighbors. The energies of the fragments were then calculated separately and compared to the energy of the cluster on the whole. The energy of the cluster on the whole subtracted from the sum of the energies of the separated fragments defines the interaction energy IE . The IE as function of the rotational angles over the range $0 \leq \theta_{\text{BH}_3} \leq 120$; $0 \leq \theta_{\text{NH}_3} \leq 120$ was expressed as:

$$IE(\theta_{\text{BH}_3}; \theta_{\text{NH}_3}) = (E_{\text{S} \rightarrow \text{E}}(\theta_{\text{BH}_3}; \theta_{\text{NH}_3}) + E_{\text{CAGE}}) - E(\theta_{\text{BH}_3}; \theta_{\text{NH}_3}),$$

where $E_{\text{S} \rightarrow \text{E}}$ is the energy calculated for an isolated molecule in the geometry of the symmetrized central AB at the respective rotational configuration (thus, represents the staggered-to-eclipsed torsion $\text{S} \rightarrow \text{E}$); E_{CAGE} is the energy of the 8 surrounding AB molecules in the geometry of the cluster; and E is the energy of the cluster on the whole. The energies were then expressed as relative

to the minimum rotational configuration **I** (the initial orientation) by subtracting the respective values calculated for $\theta_{\text{NH}_3} = 0$; $\theta_{\text{BH}_3} = 0$, thus:

$$\Delta E(\theta_{\text{BH}_3}; \theta_{\text{NH}_3}) = \Delta E_{\text{S} \rightarrow \text{E}}(\theta_{\text{BH}_3}; \theta_{\text{NH}_3}) + \Delta IE(\theta_{\text{BH}_3}; \theta_{\text{NH}_3})$$

The values of ΔE as well as the respective PES graphically depicted in Fig. 3a have been evaluated in the previous section. The values for configurations **II–IV** given in Table 1 (also discussed in the previous section) represent the barriers or activation energies. The plots of the component energies ΔIE and $\Delta E_{\text{S} \rightarrow \text{E}}$ as function of the rotational angles are shown in Fig. 3b and 3c, respectively. The torsional barrier (the maximum) for the central AB molecule isolated from the cage of 8 neighbors is 11.5 kJ mol^{-1} . The ΔIE surface, Fig. 3b, defines the rotational potential determined only by the interactions with the surrounding environment. Table 1 lists the contributions of the interaction energies to the barriers for rotation through configurations **II–IV**. Each point on the PES, Fig. 3a, can now be determined in terms of internal molecular and intermolecular interactions. In configuration **II**, the interaction energy, $\Delta IE(\theta_{\text{BH}_3} = 0; \theta_{\text{NH}_3} = 60) = 1.2 \text{ kJ mol}^{-1}$, is small such that the barrier is dominated by the barrier for molecular conformational torsion, $\Delta E_{\text{S} \rightarrow \text{E}}(\theta_{\text{BH}_3} = 0; \theta_{\text{NH}_3} = 60) = 11.5 \text{ kJ mol}^{-1}$. In configuration **III**, the central molecule is in staggered conformation such that the contribution from molecular conformational torsion is zero and the barrier is determined only by the intermolecular interaction energy, $\Delta IE(\theta_{\text{BH}_3} = 60; \theta_{\text{NH}_3} = 60) = 31.1 \text{ kJ mol}^{-1}$. In configuration **IV**, the potential from molecular conformational torsion is in the maximum, $\Delta E_{\text{S} \rightarrow \text{E}}(\theta_{\text{BH}_3} = 60; \theta_{\text{NH}_3} = 0) = 11.5 \text{ kJ mol}^{-1}$, and combines with the unfavorable intermolecular interaction energy, $\Delta IE(\theta_{\text{BH}_3} = 60; \theta_{\text{NH}_3} = 0) = 26.8 \text{ kJ mol}^{-1}$, to give the largest barrier energy of 38.3 kJ mol^{-1} .

The shape of the PES and the values of its points were understood through analysis of the interaction components in the respective geometries. The same approach was further used to compare the points of the rotational pathways on the surface. This allows examination of the competition between the molecular and

environmental forces in the correlated MEP for BH₃ rotation. In order to understand the difference between the uncorrelated and correlated rotations of BH₃, we consider transition from **IV** to **III**. The uncorrelated rotation of BH₃ has its maximum in **IV**, and the rotation of NH₃ corresponding to the transition **IV** ($\Delta IE = 26.8 \text{ kJ mol}^{-1}$) \rightarrow **III** ($\Delta IE = 31.1 \text{ kJ mol}^{-1}$) increases the *IE* component by 4 kJ mol^{-1} . The increase is due to the reorientation of the NH₃ group to a less favorable orientation with respect to the surrounding. On the other hand, in **IV**, the central AB is in an eclipsed conformation. However, the transition **IV** \rightarrow **III** restores the staggered conformation (E \rightarrow S transition), and the internal molecular component of the potential decreases by 11.5 kJ mol^{-1} . Thus, for rotation of BH₃ to **IV**, a subsequent NH₃ rotation moves the system to **III** and lowers the energy by 7 kJ mol^{-1} , which results in a decrease of the total barrier to 31.1 kJ mol^{-1} . In **IV**, the NH₃ group of the central AB is in its favorable orientation with respect to the surrounding, but the force of the molecular conformational torsion is in its maximum, thus the environment does not hold the central molecule in eclipsed conformation and the system moves to **III**. This comparison of the components of the potential energy at points **III** and **IV** suggests that the rotation of BH₃ is concomitant with NH₃ rotation and follows **I** \rightarrow **III** \rightarrow **I** rather than **I** \rightarrow **IV** \rightarrow **I** or **I** \rightarrow **IV** \rightarrow **III** \rightarrow **I**, thus, the only distinguishable rotations of AB molecule in the crystal are through points **II** and **III**.

Characterization of the rotational motions

The above approach of separating the values of the points on the PES by components from molecular and intermolecular interactions facilitates characterization of the rotational motions in the crystal of AB. Analysis of the components shows that (1) the barrier of correlated rotation is determined only by the intermolecular interactions, (2) the barrier for uncorrelated rotation of BH₃ is a combination of internal and intermolecular interactions, and (3) NH₃ rotation is dominated by internal molecular conformational forces. The energies of the interactions as function of rotational angles ($0 \leq \theta_{\text{NH}_3} \leq 120$; $0 \leq \theta_{\text{BH}_3} \leq 120$) shown on Fig. 3b and 3c support these conclusions with the positions of the respective barriers. The conclusions based on the evaluation of the components of the PES of the 9-molecule cluster show that the crystal environment has strong influence on the dynamics of BH₃ rotation in solid AB. On the other hand, the dynamics of NH₃ rotation is determined predominantly by the molecular electronic structure corresponding to the geometry of AB molecule in the crystal. The intermolecular energy surface (Fig. 3b) shows that NH₃ rotates in a smooth, nearly homogenous potential of the crystal surrounding. This observation supports the suggestion from previous experimental studies^{13–15} for nearly free rotation of NH₃. Thus, the measured value for the barrier of this rotation can be considered as a very close approximation to the barrier for molecular conformational torsion (S \rightarrow E) in the respective geometry in solid state. The molecular geometry of AB at 175 K has a shorter (1.568 Å) B–N bond, which results in an increase of the S \rightarrow E barrier to 11.5 kJ mol^{-1} (NH₃ rotational barrier measured by Penner is 13.7 kJ mol^{-1} and calculated after optimizations presented in the following section is 14.9 kJ mol^{-1}), compared to the gas phase where the B–N bond is longer (1.657 Å) and the S \rightarrow E barrier is lower 8.5 kJ mol^{-1} .⁴

Effect of geometry optimization on the barrier heights

The cluster model presented here mimics the crystal arrangement by fixing the surrounding and the geometry of the central AB molecule. Because the rotational trajectories are determined by the fixed hydrogen positions of the central AB, the rotations are also restricted. These restrictions may not allow accurate accounting for lattice effects on the rotational dynamics. In an attempt to test this hypothesis, the energies for configurations **I–III** and the respective barriers (**II** and **III**) were recalculated by increasing the number of relaxed hydrogen atoms in the frame of fixed boron and nitrogen positions. First, the effect of the dihydrogen bonding was examined by relaxing the hydrogen atoms involved in forming the 6 dihydrogen bonds. This approach actually results in greater discrepancy with the experiment giving barriers of 34.0 and 15.1 kJ mol^{-1} for BH₃ and NH₃ rotation, respectively (Table 1). In the geometries of optimized dihydrogen bonding of the central AB in the configuration **III**, the shortest dihydrogen contact for the central BH₃ group is 1.37 \AA , while for the NH₃ group, **II** is 2.00 \AA . Further, a relaxation of all hydrogen positions in **I–III** was performed in a setting such that allows reorientation about B–N bonds of all neighboring molecules, but the central one. Even when all hydrogen atoms in the 9-molecule cluster are relaxed, the barriers are still significantly greater than those seen in the experiment, 35.6 kJ mol^{-1} for the BH₃ rotation and 14.9 kJ mol^{-1} for NH₃ rotation. This result suggests that the boron and nitrogen atoms of the neighboring molecules are also involved in the dynamics of the intermolecular interactions in the solid. Specifically, the response of the lattice includes not only motions of the hydrogen atoms but the whole molecules of the surrounding. Such a conclusion about the role of the lattice in the dynamics of AB is consistent with the “wobbling” motion about B–N axis described by Reynhard and Hoon for the orthorhombic phase in their NMR experimental work.^{13b}

MP2 calculations of the barrier heights

In an attempt to elucidate the difference between the calculated and measured values of the correlated BH₃ barrier, a comparison to MP2 calculations in the same basis set was performed. The barriers were recalculated for configurations **I–IV** with no optimization and the results are listed in Table 1. The MP2 calculated barriers of BH₃ rotation (36.0 kJ mol^{-1} , correlated and 44.8 kJ mol^{-1} , uncorrelated) are higher than the corresponding B3LYP values. However, the MP2 calculated barrier of NH₃ rotation (12.7 kJ mol^{-1}) agrees with both the corresponding B3LYP and the NMR experimental value. The barriers for rotations involving BH₃ calculated at B3LYP and MP2 levels do not agree as well with the experiment. This is probably due to deficiencies in the cluster model rather than the level of theory.

Nature of the intermolecular components of the rotational barriers

The evaluation of the barrier heights and the analysis of molecular and environmental components of the energy potential for rotational motion in solid AB show that the barriers depend on the intermolecular dihydrogen contact distances in configurations **I–IV** (Fig. 2 planar representations). The higher barrier for BH₃ rotation may be due to a short, repulsive dihydrogen contact (1.43 \AA) in configurations **III** and **IV** (Fig. 2), as compared

Table 2 Energy decomposition analysis of minimum and maximum energy configurations for rotational motion of the central AB molecule in a 9-molecule cluster at RHF/6–31G level of theory. The components of the energies in kJ mol⁻¹: electrostatic (ES), exchange (EX), repulsion (PL), charge transfer (CT), and other (MIX)

	ES	EX	PL	CT	MIX	Total
I	-37.95	82.64	-13.89	-22.12	2.26	10.94
II	-32.62	75.13	-12.99	-20.13	1.43	10.83
III	-57.69	161.99	-27.82	-43.00	17.75	51.24
IV	-63.73	169.06	-29.32	-44.96	18.58	49.64

with lower barrier for NH₃ rotation where there is little change in the dihydrogen contact (2.07 Å) in configuration **II** (Fig 2). To test the hypothesis of repulsive interactions as a function of dihydrogen bond distance, an EDA as developed by Morokuma and coworkers^{29a} was applied. The EDA provides a mechanism to separate the intermolecular interactions into the specific electrostatic (ES), polarization (PL), charge transfer (CT), and exchange repulsion (EX) energy components. For detailed definition of these terms, refer to the original papers. The EDA results for configurations **I–IV** are listed in Table 2 and show that exchange repulsion contributes most significantly to the BH₃ rotational barrier. This is consistent with chemical intuition once we observe that two hydrogen atoms of the BH₃ end of the central AB are within 1.43 Å from the closest hydrogen atoms of neighboring NH₃ groups (configurations **III** and **IV**, Fig 2). While such a close distance results in larger attractive (more negative) ES, PL, and CT components of the interaction energy compared to configuration **I**, this close distance results in an even larger increase of the EX repulsion such that the overall interaction energies in **III** and **IV** are unfavorable. In the NH₃ uncorrelated rotation configuration **II** (where BH₃ is in favorable orientation with respect to the surrounding), the shortest distance to hydrogen atoms of neighboring BH₃ groups is 2.07 Å. This molecular orientation results in much smaller difference of the stabilization compared to the repulsion forces and thus a smaller *IE* contribution and smaller barrier. The results for the balance of the interaction energy components for the configurations **II–IV** and the respective barriers are consistent with the description of the radial dependence of EX for AB donor–acceptor complex by Mo and coworkers.¹² The shortest dihydrogen bond in **III** and **IV** (1.43 Å) is in the region of fast growing of EX. while in **II**, the shortest dihydrogen bond (2.07 Å) is in the region where EX is comparable with the stabilization components. Note that for isolated AB molecule, EX is the interaction controlling the barrier of molecular conformational torsion (S → E). This was found by theoretical studies applying various decomposition schemes for the interaction of BH₃ with NH₃ in AB molecule.^{10,11,30} These studies have shown that the internal rotational dynamics and the E → S barrier are controlled predominantly by the exchange repulsion.

In this work, an EDA of the “first neighbors” cluster model applied for single molecule rotation shows that the molecular geometry, e.g., the longer B–H bonds (1.14 Å), relative to the shorter N–H bonds (0.96 Å) and the specific molecular orientation in the crystal result in higher steric repulsion and consequently a higher barrier for BH₃ rotation compared to NH₃ rotation. For both rotations, exchange repulsion controls the barrier heights.

For BH₃, this is the EX of the intermolecular interactions as a result of short dihydrogen contacts in the region of fast-growing repulsion, while for NH₃, it originates from the internal molecular interactions.

Conclusions

The transition from high-temperature tetragonal phase to low-temperature orthorhombic phase of AB leads to a tilting (deviation) of the B–N bonds away from parallel with the *c* axis of the unit cell. The effect of this rearrangement on the dynamics is that there is no longer only a single “whole molecule” reorientation as noted by previous studies,^{13–15,31} but the rotational motion is split into two distinguishable rotations: uncorrelated NH₃ and correlated BH₃–NH₃ rotation. In the orthorhombic phase, the two ends of the molecule are not equivalent in terms of molecular and crystal geometry, which leads to changes in the dihydrogen bonding interactions. The computational model based upon single molecule rotation in the presence of a fixed cage of neighboring AB molecules provides unique insight into the environmental parameters that effect rotational dynamics. The calculated barrier for NH₃ rotation (12.7 kJ mol⁻¹) is in agreement with the experimental barrier (average of the reported values^{13–15} of 12.6 ± 2.6 kJ mol⁻¹). We find that the barrier for the correlated rotation of BH₃ with NH₃ (whole molecule rotation, 31.7 kJ mol⁻¹) is significantly lower than the barrier for uncorrelated BH₃ rotation (38.3 kJ mol⁻¹) but greater than the experimental rotational barrier (26 kJ mol⁻¹). The NH₃ rotational barrier is determined by internal molecular repulsion of the staggered conformation and is little influenced by surrounding AB molecules. This is very different for the BH₃ rotational barrier where repulsion from dihydrogen bonding interactions with neighboring AB molecules plays an important role and rules out the independent mode. More advanced modeling that includes intermolecular correlated motions (lattice breathing) to permit spatial and conformational adjustments is planned to further study the role of intermolecular correlated motion in the molecular crystal AB.

Acknowledgements

Support for this work by the US Department of Energy, Office of Science, Basic Energy Sciences, Chemical Sciences Division is gratefully acknowledged. Pacific Northwest National Laboratory is operated by Battelle for the US Department of Energy.

References

- (a) F. Baitalow, J. Baumann, G. Wolf, K. Jaenicke-Röbler and G. Leitner, *Thermochim. Acta*, 2002, **391**, 159; (b) A. Gutowska, L. Li, Y. Shin, C. M. Wang, X. S. Li, J. C. Linehan, R. S. Smith, B. D. Kay, B. Schmid, W. Shaw, M. Gutowski and T. Autrey, *Angew. Chem., Int. Ed.*, 2005, **44**, 3578; (c) M. E. Bluhm, M. G. Bradley, R. Butterick III, U. Kusari and L. G. Sneddon, *J. Am. Chem. Soc.*, 2006, **128**, 7748; (d) F. H. Stephens, V. Pons and R. T. Baker, *Dalton Trans.*, 2007, 2613–2626; (e) T. B. Marder, *Angew. Chem., Int. Ed.*, 2007, **46**, 8116.
- S. G. Shore and R. W. Parry, *J. Am. Chem. Soc.*, 1955, **77**, 6084.
- A. Haaland, *Angew. Chem., Int. Ed. Engl.*, 1989, **28**, 992.
- L. R. Thorne, R. D. Suenrum and F. J. Lovas, *J. Chem. Phys.*, 1983, **78**, 167.
- W. T. Klooster, T. F. Koetzle, P. E. M. Siegbahn, R. B. Richardson and R. H. Crabtree, *J. Am. Chem. Soc.*, 1999, **121**, 6337.

- 6 C. A. Morrison and M. M. Siddick, *Angew. Chem., Int. Ed.*, 2004, **43**, 4780.
- 7 (a) J. Baumann, Ph.D. Thesis, TU Bergakademie Freiberg, Germany, 2003; (b) D. A. Dixon and M. Gutowski, *J. Phys. Chem. A*, 2005, **109**, 5129; (c) M. H. Matus, K. D. Anderson, D. M. Camaioni, T. Autrey and D. A. Dixon, *J. Phys. Chem. A*, 2007, **111**, 4411.
- 8 E. R. Alton, R. D. Brown, J. C. Carter and R. C. Taylor, *J. Am. Chem. Soc.*, 1959, **81**, 3550.
- 9 For a review see: (a) W. Grochala and P. P. Edwards, *Chem. Rev.*, 2004, **104**, 1283; (b) For specific examples see: A. C. Stowe, W. J. Shaw, J. C. Linehan, B. Schmid and T. Autrey, *Phys. Chem. Chem. Phys.*, 2007, **9**, 1831; (c) P. Chen, Z. Xiong, J. Luo, J. Lin and K. L. Tan, *Nature*, 2002, **420**, 302; (d) X. B. Zhang, S. Q. Shi, L. Jiang, S. Han, Y. Kotani, T. Kiyobayashi, N. Kuriyama, T. Kobayashi and Q. Xu, *J. Phys. Chem. C*, 2007, **111**, 5064.
- 10 P. R. Schreiner, *Angew. Chem., Int. Ed.*, 2002, **41**, 3579.
- 11 H. Umeyama and K. Morokuma, *J. Am. Chem. Soc.*, 1976, **98**, 7208.
- 12 Y. Mo, L. Song, W. Wu and Q. Zhang, *J. Am. Chem. Soc.*, 2004, **126**, 3974.
- 13 (a) E. L. Lippert and W. N. Lipscomb, *J. Am. Chem. Soc.*, 1956, **78**, 503; (b) F. Borsa, A. Rigamonti, *Magnetic Resonance of Phase Transitions*, ed. F. J. Owens, C. P. Poole and H. A. Farach, 1979, New York, Academic Press, pp. 79–165.
- 14 (a) C. F. Hoon and E. C. Reynhardt, *J. Phys. C: Solid State Phys.*, 1983, **16**, 6129; (b) E. C. Reynhardt and C. F. Hoon, *J. Phys. C: Solid State Phys.*, 1983, **16**, 6137.
- 15 G. H. Penner, Y. C. Phillis Chang and J. Hutzal, *Inorg. Chem.*, 1999, **38**, 2868.
- 16 (a) O. Gunaydin-Sen, R. Achey, N. S. Dalal, A. Stowe and T. Autrey, *J. Phys. Chem. B*, 2007, **111**, 677; (b) H. Cho, W. J. Shaw, V. M. Parvanov, G. K. Schenter, A. Karkamkar, N. J. Hess, C. Mundy, S. Kathmann, J. Sears, A. S. Lipton, P. D. Ellis and T. Autrey, *J. Phys. Chem. A*, 2008, **112**, 4277; (c) N. J. Kress, M. R. Hartman, C. M. Brown, E. Mamontov, A. Karkamkar, D. J. Heldebrant, L. L. Daemen and T. Autrey, *Chem. Phys. Lett.*, 2008, **459**, 85.
- 17 The temperature of 175 K is the median of the experimental temperature range used by Penner *et al.* to measure the rotational barrier of AB in the orthorhombic phase.
- 18 H. I. Schlesinger, H. C. Brown, D. L. Mayfield and J. R. Gilbreath, *J. Am. Chem. Soc.*, 1953, **75**, 213.
- 19 G. W. Schaeffer and E. R. Anderson, *J. Am. Chem. Soc.*, 1949, **71**, 2143.
- 20 R. E. Davis, A. E. Brown, R. Hopmann and C. L. Kibby, *J. Am. Chem. Soc.*, 1963, **85**, 487.
- 21 M. G. Hu, J. M. Van Paasschen and R. A. Geangel, *J. Inorg. Nucl. Chem.*, 1977, **39**, 2147.
- 22 (a) H. M. Rietveld, *Acta Crystallogr.*, 1967, **22**, 151; (b) H. M. Rietveld, *J. Appl. Crystallogr.*, 1969, **2**, 65.
- 23 B. H. Toby, *J. Appl. Crystallogr.*, 2001, **34**, 210.
- 24 A. D. Becke, *J. Chem. Phys.*, 1993, **98**, 5648.
- 25 (a) W. J. Hehre, R. Ditchfield and J. A. Pople, *J. Chem. Phys.*, 1972, **56**, 2257; (b) J. D. Dill and J. A. Pople, *J. Chem. Phys.*, 1975, **62**, 2921; (c) M. M. Francl, W. J. Pietro, W. J. Hehre, J. S. Binkley, M. S. Gordon, D. J. DeFrees and J. A. Pople, *J. Chem. Phys.*, 1982, **77**, 3654.
- 26 *Gaussian 98, Revision A.7*, M. J. Frisch, G. W. Trucks, H. B. Schlegel, G. E. Scuseria, M. A. Robb, J. R. Cheeseman, V. G. Zakrzewski, J. A. Montgomery, Jr., R. E. Stratmann, J. C. Burant, S. Dapprich, J. M. Millam, A. D. Daniels, K. N. Kudin, M. C. Strain, O. Farkas, J. Tomasi, V. Barone, M. Cossi, R. Cammi, B. Mennucci, C. Pomelli, C. Adamo, S. Clifford, J. Ochterski, G. A. Petersson, P. Y. Ayala, Q. Cui, K. Morokuma, D. K. Malick, A. D. Rabuck, K. Raghavachari, J. B. Foresman, J. Cioslowski, J. V. Ortiz, A. G. Baboul, B. B. Stefanov, G. Liu, A. Liashenko, P. Piskorz, I. Komaromi, R. Gomperts, R. L. Martin, D. J. Fox, T. Keith, M. A. Al-Laham, C. Y. Peng, A. Nanayakkara, C. Gonzalez, M. Challacombe, P. M. W. Gill, B. Johnson, W. Chen, M. W. Wong, J. L. Andres, C. Gonzalez, M. Head-Gordon, E. S. Replogle and J. A. Pople, Gaussian, Inc., Pittsburgh, PA, 1998.
- 27 M. W. Schmidt, K. K. Baldrige, J. A. Boatz, S. T. Elbert, M. S. Gordon, J. H. Jensen, S. Koseki, N. Matsunaga, K. A. Nguyen, S. Su, T. L. Windus, M. Dupuis and J. A. Montgomery, *J. Comput. Chem.*, 1993, **14**, 1347.
- 28 These subtle changes are expected based upon the change in lattice parameters noted by Reinhardt. The B–N tilting is unique to the orthorhombic phase and doesn't exist in tetragonal phase, where $a = b$ and all B–N are parallel to the c axis.
- 29 (a) K. Kitaura, S. Sakaki and K. Morokuma, *Inorg. Chem.*, 1981, **20**, 2292; (b) K. Morokuma, K. Kitaura, *Chemical Applications of Atomic and Molecular Electrostatic Potentials*, Plenum Press, 1981; (c) G. Frenking and N. Frohlich, *Chem. Rev.*, 2000, **100**, 717.
- 30 A. Jagielska, R. Moszynski and L. Piela, *J. Chem. Phys.*, 1999, **110**, 947.
- 31 J. Dillen and P. Verhoeven, *J. Phys. Chem. A*, 2003, **107**, 2570.